DALTON
FULL PAPER

Response to steric constraint in azacryptate and related complexes of iron-(II) and -(III)*

F. Anthony Deeney,[a] Charles J. Harding,[b] Grace G. Morgan,[c] Vickie McKee,[c] Jane Nelson,[b,c] Simon J. Teat[d,e] and William Clegg[d,e]

[a] *Physics Department, University College, Cork, Ireland*
[b] *Chemistry Department, Open University, Milton Keynes, UK MK7 6AA*
[c] *School of Chemistry, Queen's University, Belfast, UK BT9 5AG*
[d] *CLRC, Daresbury Laboratory, Daresbury, Warrington, Cheshire, UK WA4 4AD*
[e] *Department of Chemistry, University of Newcastle, Newcastle upon Tyne, UK NE1 7RU*

Iron(II) cryptates, where the Fe^{II} is in the high-spin $S = 2$ electronic configuration, even with six sp^2 N-donors, and iron(III) cryptates adopting the intermediate spin $S = \frac{3}{2}$ state have been prepared. The structure of a high-spin iron(II) cryptate utilising six sp^2 N-donors shows long metal–ligand distances which effectively destabilise the low-spin ^1A_g configuration. Comparison is made between iron(III) cryptates, a less sterically constrained podand complex of the same donor set, and analogous $N_4O^-_2$ polychelates, which are respectively intermediate-, high- and low-spin or $S = \frac{5}{2} \longleftrightarrow S = \frac{1}{2}$ spin crossover systems. The Mössbauer spectra of the iron(III) cryptates and analogous podate are remarkably similar, despite their different spin states, suggesting covalency in the podate binding. The crystal structure of the podate supports this conclusion, as the iron–ligand donor distances are short for high-spin Fe^{III}.

Although iron cations have been frequently used as template ions in macrocyclic chemistry,[1] there are only a few examples[2,3] of their incorporation within macrobicyclic or cryptand ligands. Polyether cryptands do not in general constitute sufficiently strong ligands for transition cations to compete successfully with co-ordinating solvents, and there have as yet been only a few reports[4,5] of iron complexation with the potentially more suitable azacryptand hosts. This is at least partly because of the strong Lewis acid nature of the normally stable iron(III) redox state which can result either in metal-assisted hydrolytic attack on the ligand[6] (in the case of imino-cryptands) or unsuccessful competition with protonation[4b,5] (in the case of amino-cryptands).

However, certain specific properties of iron cryptates make a well directed synthetic effort towards their isolation and characterisation worthwhile. The elucidation of the structure and function of non-heme oxidases such as hemerythrin[7] and related systems has stimulated interest in sterically protected diiron(II) systems, in the hope that they might be able to stabilise partly reduced dioxygen intermediates within the sterically protected cavity. Sequestration[8] of the potentially toxic iron(III) cation is of medical importance in connection with iron decorporation pharmaceuticals for use in iron-excess pathology, as in thalassemia and other diseases of iron metabolism. There is interest also in the ability of cage ligands to control redox stability *via* tuning of both the nature and geometric disposition[9] of the donor set. From a materials science point of view the study of spin state control *via* geometry is likewise of importance because of potential applications in, for example, optical information technology.[10]

We have available[11] a range of possible hosts for iron: these include azacryptands with charge-neutral imino- and amino-N-donors, or potentially anionic iminophenolate cryptands, which offer the chance to utilise either one or a pair of co-ordination sites in the generation of mono- or di-nuclear cryptates. In order to monitor the effect of steric constraint on spin and redox state, we have also studied analogous podand or polychelating acyclic ligands where steric effects are expected to be absent or much reduced.

On the usual hard–soft acid–base considerations the neutral imino-ligands may be expected to stabilise Fe^{II} although there may be some possibility of ligand degradation *via* metal-assisted hydrolytic processes. Neutral amino-ligands are not expected to be susceptible to hydrolysis but are expected to favour, to some extent, the higher +III redox state. The potentially anionic iminophenolate systems, whether macrobicyclic or acyclic should, on electrostatic grounds, favour iron(III) encapsulation. We here report the magnetic, ESR spectroscopic and Mössbauer properties of mono- and di-iron complexes of this range of ligands, in both common redox states, to illustrate the effect of geometry on redox and spin state stabilisation across the series.

Results and Discussion

Monoiron(II) cryptate $[FeL^1][ClO_4]_2$

As anticipated, the +II redox state was most easily obtained using the pyridine-based iminocryptand L^1, which can offer six sp^2 N-donors to the iron(II) cation. The mononuclear 1:1 iron(II) cryptate $[FeL^1][ClO_4]_2$ **1** shows a normal, nearly temperature-independent moment for high-spin iron(II) instead of the expected[12] low-spin magnetic moment (Table 1). When 2:1 Fe:ligand stoichiometry was used, however, a poorly characterised purple (probably ring-opened) product was obtained together with **1**, the impure samples showing reduced paramagnetism. In the L^1 series it is noticeable that only copper[13,14] shows any tendency to form intact dinuclear cryptates; other transition series cations show metal-assisted ring opening in their dinuclear products of reaction with this cryptand. Complex **1** has a normal high-spin $S = 2$ Mössbauer spectrum[15] (Table 2) but samples contaminated with the purple ring-opened product show a second broad, unsplit Mössbauer feature around isomer shift $\delta = -0.1$ mm s^{-1} *vs.* Fe, consistent with a low-spin iron(II) impurity.

Adoption of the high-spin $^5T_2$ state in complex **1**, given the relatively strong field donors used, is presumed to derive from

* *Supplementary data available*: magnetic susceptibility data. For direct electronic access see http://www.rsc.org/suppdata/dt/1998/1837/, otherwise available from BLDSC (No. SUP 57377, 8 pp.) or the RSC Library. See Instructions for Authors, 1998, Issue 1 (http://www.rsc.org/dalton). *Non-SI units employed*: $\mu_B \approx 9.27 \times 10^{-24}$ J T^{-1}, Ci = 3.7×10^{-10} Bq.

Table 1 Magnetic, ESR and electronic spectral properties of iron complexes

Complex	Colour	μ/μB 80 K	μ/μB 300 K	g[a]	λmax/10³ cm⁻¹ (ε/10³ dm³ mol⁻¹ cm⁻¹)[b]
1 $[FeL^1][ClO_4]_2$	Brownish pink	5.27	5.36	—	20.9 (2.0), 33.4 (≈30)
2a $[Fe_2(N_3)L^2][CF_3SO_3]_3\cdot 2H_2O$	Cream	4.55	5.26	—	*c*
2a′ $[Fe_2(N_3)L^2][ClO_4]_3\cdot 2H_2O$	Cream	4.28[d]	4.97		*c*
2b $[Fe_2(OH)L^2][PF_6]_3\cdot 4H_2O$	Cream	3.20	4.71	—	*c*
3 $[Fe_2(OH)L^3][CF_3SO_3][BPh_4]_2$	Cream	2.91	4.51	—	*c*
4a $[FeL^4][ClO_4]_3\cdot 0.5MeCN$	Dark green	4.12[d]	4.08	7.2s, ≈4.2ms (br), ≈2.1w (br),	18.4 (3.7), 26.8 (19.7)
4b $[FeL^4][BF_4]_3\cdot 6H_2O$	Olive green	5.89	5.67	6.1m, 4.3m (br), 2.20s	17.0 (sh), 24.4 (51.8), 37 (≈60)
4c $[FeL^4][CF_3SO_3]_3\cdot 3H_2O$	Purple		6.2	—	—
5 $[FeL^5][ClO_4]_3\cdot EtOH$	Dark green	3.65[d]	3.48	7.6ms, 4.2s, ≈2.2vw (br)	18.0 (1.8), 21.8 (6.1), 28.4 (11.6)
6 $[FeL^6]\cdot 0.75MeCN\cdot 0.125H_2O$	Maroon	5.87	6.02	4.2,[e] ≈2w[e]	21.3 (4.8), 23.9 (4.6), 37 (≈14)
7 $[FeL^7][CF_3SO_3]$	Purple	1.99	2.13	2.35, 2.12, 1.96	17.9 (2.7), 25 (4.7), 29 (6.7)
8 $[FeL^8][ClO_4]\cdot 3H_2O$	Purple	3.35[d]	4.10	4.3w, 2.13s	15.7 (0.7), 24.7 (5.5), 29.4 (12.6)

[a] Polycrystalline, −160 °C; s = strong, m = medium; w = weak; v = very; br = broad. [b] In MeCN. [c] Air sensitivity prevented acquisition of reliable spectra. [d] μ at 4 K: **2a**, 2.89; **4a**, 4.04; **5**, 3.33; **8**, 2.74 μB. [e] dmf glass spectrum, −160 °C.

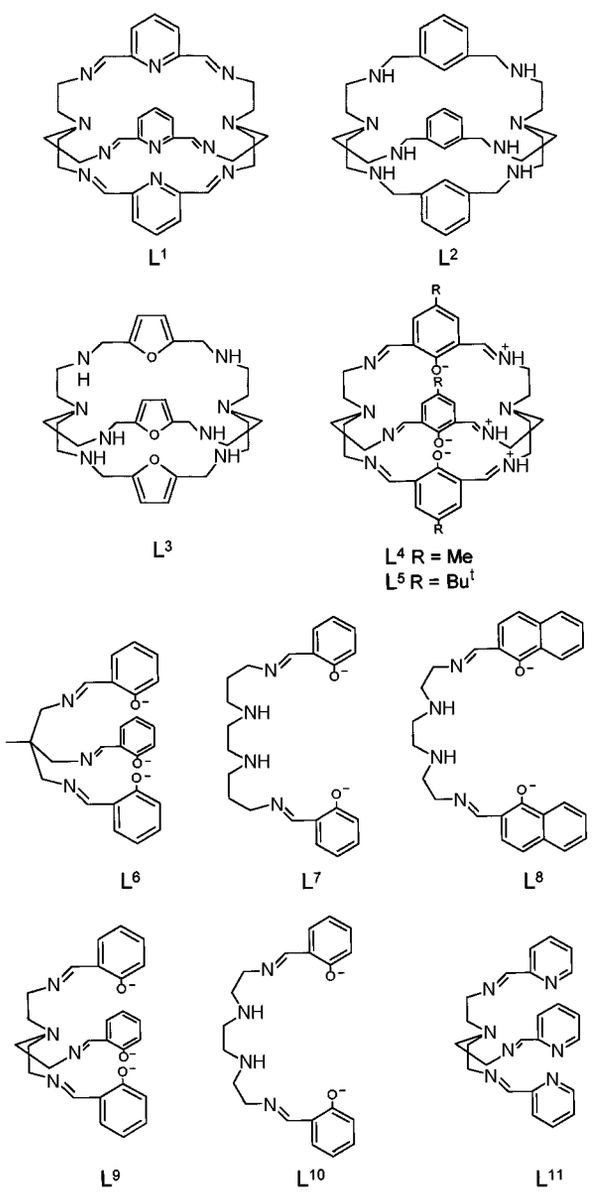

the geometric constraints of the cryptand co-ordination site. Were a regular, and appropriately sized, octahedral site available its utilisation would generate the stable spin-paired configuration common in iron(II) complexes of sp^2 N-donor ligands, which are in general resistant to the aerobic oxidation affecting high-spin iron(II) complexes. Complex **1** is insensitive to aerobic oxidation, despite its high-spin configuration,

Table 2 Mössbauer parameters for iron complexes

Complex	295 K δ[a]/mm s⁻¹	295 K ΔE[b]/mm s⁻¹	80 K δ[a]/mm s⁻¹	80 K ΔE[b]/mm s⁻¹
1	0.99	1.06	1.11	1.41
2a	0.85 (br)	1.72 (br)	*c*	*c*
2b	1.12	1.00	*d*	*d*
3	1.08	1.98	*d*	*d*
4a	0.44 (br)	0.67 (br)	0.51	0.64
4b	0.38	0.63	0.45	0.65
5	≈0.3	vbr, unsplit	≈0.3	vbr, unsplit
6	0.39	unsplit	0.45	unsplit
7	0.16	2.09	0.17	2.87
8	0.38[e]	0.81[e]	0.50[f]	0.81[f]
	0.12[f]	2.48[f]	0.20[e]	2.61[e]

[a] *vs.* Iron metal, ±0.02 mm s⁻¹ (except where broad). [b] ±0.03 mm s⁻¹ (except where broad). [c] Broad complex spectrum. [d] Not measured. [e] Major component. [f] Minor component.

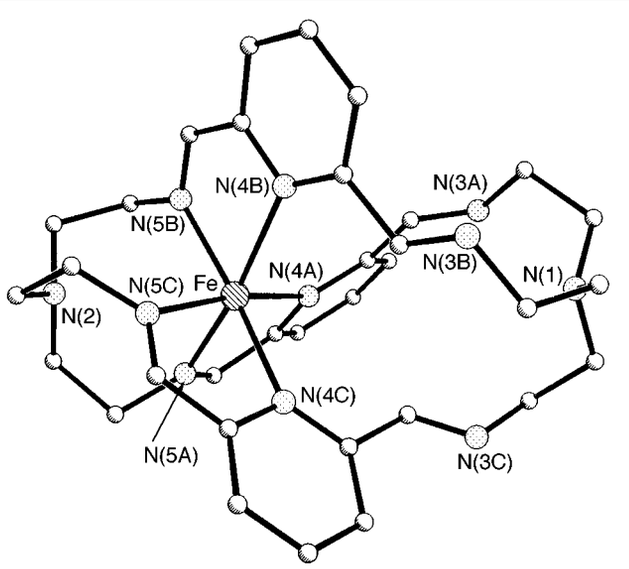

Fig. 1 Perspective view of the $[FeL^1]^{2+}$ cation. Hydrogen atoms are omitted for clarity

perhaps because of kinetic stability towards decomplexation. The geometry which makes dinuclearity unlikely within this host is illustrated by the crystal structure of **1**·MeCN.

The cation is shown in Fig. 1, selected bonds and angles are included in Table 3. The iron(II) ion is located towards one end of the cryptand cavity and is co-ordinated to three imine and three pyridyl nitrogen donors. There are no significant interactions between the cation and the perchlorate anions or the solvate molecule. The geometry at the iron is twisted by 10°

Table 3 Selected bond lengths (Å) and angles (°)

$[FeL^1][ClO_4]_2$·MeCN **1**·MeCN			
Fe–N(5B)	2.128(3)	Fe–N(5A)	2.143(3)
Fe–N(5C)	2.145(2)	Fe–N(4C)	2.308(3)
Fe–N(4A)	2.321(2)	Fe–N(4B)	2.337(2)
N(5B)–Fe–N(5A)	85.5(1)	N(5B)–Fe–N(5C)	94.6(1)
N(5A)–Fe–N(5C)	94.5(1)	N(5B)–Fe–N(4C)	169.0(1)
N(5A)–Fe–N(4C)	88.9(1)	N(5C)–Fe–N(4C)	75.0(1)
N(5B)–Fe–N(4A)	87.8(1)	N(5A)–Fe–N(4A)	75.2(1)
N(5C)–Fe–N(4A)	169.6(1)	N(4C)–Fe–N(4A)	103.1(1)
N(5B)–Fe–N(4B)	74.9(1)	N(5A)–Fe–N(4B)	170.2(1)
N(5C)–Fe–N(4B)	88.1(1)	N(4C)–Fe–N(4B)	100.8(1)
N(4A)–Fe–N(4B)	102.3(1)		
$[FeL^6]$·0.75MeCN·0.125H_2O **6**·0.75MeCN·0.125H_2O			
Fe(1)–O(1A)	1.957(2)	Fe(2)–O(1D)	1.945(2)
Fe(1)–O(1B)	1.936(2)	Fe(2)–O(1E)	1.940(2)
Fe(1)–O(1C)	1.938(2)	Fe(2)–O(1F)	1.947(2)
Fe(1)–N(1A)	2.159(2)	Fe(2)–N(1D)	2.160(2)
Fe(1)–N(1B)	2.147(2)	Fe(2)–N(1E)	2.156(2)
Fe(1)–N(1C)	2.143(2)	Fe(2)–N(1F)	2.132(2)
O(1B)–Fe(1)–O(1A)	96.99(7)	O(1E)–Fe(2)–O(1D)	93.46(8)
O(1C)–Fe(1)–O(1A)	94.06(7)	O(1D)–Fe(2)–O(1F)	93.70(7)
O(1B)–Fe(1)–O(1C)	96.18(7)	O(1E)–Fe(2)–O(1F)	95.50(8)
O(1A)–Fe(1)–N(1A)	84.80(7)	O(1D)–Fe(2)–N(1D)	85.12(8)
O(1A)–Fe(1)–N(1B)	95.91(8)	O(1D)–Fe(2)–N(1E)	95.81(8)
O(1A)–Fe(1)–N(1C)	165.60(7)	O(1D)–Fe(2)–N(1F)	166.87(8)
O(1B)–Fe(1)–N(1A)	169.21(7)	O(1E)–Fe(2)–N(1D)	165.62(8)
O(1B)–Fe(1)–N(1B)	85.74(7)	O(1E)–Fe(2)–N(1E)	85.01(8)
O(1B)–Fe(1)–N(1C)	97.26(8)	O(1E)–Fe(2)–N(1F)	99.62(8)
O(1C)–Fe(1)–N(1A)	94.30(8)	O(1F)–Fe(2)–N(1D)	98.87(8)
O(1C)–Fe(1)–N(1B)	169.54(8)	O(1F)–Fe(2)–N(1E)	170.43(8)
O(1C)–Fe(1)–N(1C)	86.44(7)	O(1F)–Fe(2)–N(1F)	86.09(8)
N(1B)–Fe(1)–N(1A)	83.50(8)	N(1E)–Fe(2)–N(1D)	80.9(1)
N(1C)–Fe(1)–N(1A)	80.81(8)	N(1F)–Fe(2)–N(1D)	81.95(8)
N(1C)–Fe(1)–N(1B)	83.11(8)	N(1F)–Fe(2)–N(1E)	84.40(8)

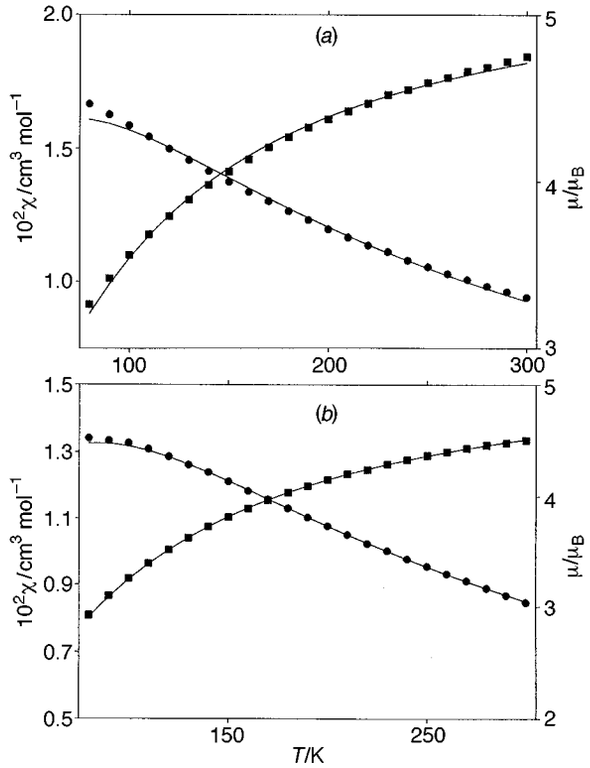

Fig. 2 Temperature dependence of the magnetic susceptibility (●) and magnetic moment (■) per Fe for the μ-hydroxo-bridged diiron cryptates (*a*) **2b** and (*b*) **3**. Solid lines represent best fits of the exchange equation for the spin Hamiltonian $H = -2JS_1 \cdot S_2$ for $S_1 = S_2 = 2$ using equation (1). For complex **2b**, $-2J = 23$ cm^{-1}, $g = 2.16$, $N_\alpha = 300 \times 10^{-6}$ cm^3 mol^{-1}. For complex **3**, $-2J = 27$ cm^{-1}, $g = 2.13$, $N_\alpha = 80 \times 10^{-6}$ cm^3 mol^{-1}

from regular octahedral, only 4° greater than the twist (φ) in the corresponding low-spin complexes[16,17] of the podand L^1[11]. The most notable feature of the cryptate structure is the difference between the iron–imine bonds (mean 2.14 Å) and the very long iron–pyridyl N distances (mean 2.32 Å). This difference is not reproduced in the related podand complexes and is attributed to the steric constraints of the closed cryptand ligand. It is tempting, therefore, to ascribe the high-spin state of this complex to the relatively large cavity which would disfavour the smaller low-spin iron(II) ion. Low-spin iron(II) complexes with conjugated pyridine systems may show iron–pyridyl and –imine distances as short as 1.84 and 1.90 Å, respectively.[18]

Diiron(II) cryptates of L^2 and L^3

The other neutral ligands used in this study, L^2 and L^3, are amino-cryptands, where the 'harder' sp^3 N-donors cannot be expected to favour the iron(II) redox state as strongly as in L^1. Good anaerobic atmospheric protection is therefore essential for the iron(II) encapsulation reaction; this resulted in formation of diiron(II) cryptates, $[Fe_2(OH)L^2][PF_6]_3$·4H_2O **2b** and $[Fe_2(OH)L^3][CF_3SO_3][BPh_4]_2$ **3** where the co-ordination sphere of Fe^{II} is completed *via* μ-hydroxo links in the absence of other deliberately added bridging anions. Where other anions are present they can replace the hydroxide ligand. For example, the pseudo-halide anion, azide, generates a μ-azido diiron cryptate $[Fe_2(N_3)L^2][CF_3SO_3]_3$·2$H_2O$ **2a**, where the anomalously high $\nu_{asym}(N_3^-)$ infrared absorption frequency (2192 cm^{-1})[5,19] implies adoption of collinear M–NNN–M geometry. It is unsurprising in this case, given the utilisation of only five N-donors, and these being of weaker field than the six sp^2 donors used in L^1, to find Fe^{II} in a high-spin electronic configuration.

Extrapolating from the structurally well characterised dicopper(II) analogues,[11,19,20] the diiron(II) cryptates of L^2 and L^3 are expected to have co-ordination sites separated by around 4 Å for hydroxo- and 6 Å in the linear azido-bridged cryptate. At these distances, interaction may be expected between the encapsulated paramagnetic cations. The magnetic moments of both μ-hydroxo-diiron(II) cryptates **2b** and **3** do fall significantly with temperature, and susceptibility data can be satisfactorily fitted (Fig. 2) by the exchange equation (1) for the spin Hamiltonian $H = -2JS_1 \cdot S_2$ for $S_1 = S_2 = 2$ using $-2J$ values of 23 and 27 cm^{-1} respectively, indicating a similar degree of interaction to that found in other diiron(II) complexes[21] and indeed in deoxyhemerythrin itself. However the azido derivatives show virtually no interaction ($-2J = 9$ and 2.6 cm^{-1} respectively for the triflate and perchlorate salts **2a** and **2a′**). This is explained by the good fit of linearly bridging azide within the site offered by our diiron cryptate host which ensures replacement of μ-hydroxo by μ-1,3-azido, in contrast to the natural site where the bridging ligand in the azido derivative remains hydroxo. Other 1,3-azido bridges collinearly co-ordinated within the cryptate cavity provided by a pair of later first series transition cations show[22] magnetic interaction ranging from weak antiferromagnetic [typified by dimanganese(II)] to weak ferromagnetic [typified by dinickel(II) and dicopper(II)].

Mössbauer parameters for the complexes are given in Table 2. The iron(II) cryptates show the relatively large isomer shifts and quadrupole splittings expected[15] of the high-spin $S = 2$ state. As expected, none of the iron(II) systems shows ESR activity.

$$\chi_m = \left(\frac{Ng^2\mu_B^2}{kT}\right) \times \left[\frac{2\exp(2J/kT) + 10\exp(6J/kT) + 28\exp(12J/kT) + 60\exp(20J/kT)}{1 + 3\exp(2J/kT) + 5\exp(6J/kT) + 7\exp(12J/kT) + 9\exp(20J/kT)}\right] + N_\alpha \quad (1)$$

Mononuclear iron(III) iminophenolate systems

With ligands of the phenolate series the expected stable redox state is +III because of the anionic nature of the ligand which readily deprotonates on co-ordination. As established by NMR spectroscopy[11b] for main group mononuclear cryptates, each phenolic proton consequently transfers to the unco-ordinated imine. The intensely coloured mononuclear iron(III) cryptates **4a**, **4b** and **5** were obtained, irrespective of stoichiometry, on iron-(II) or -(III) transmetallation of the appropriate sodium cryptate. Despite the presence of a pair of putative co-ordination sites no diiron complexes were obtained. It is tempting to attribute this fact to electrostatic effects, given the considerable tendency[4b,9] of the isoelectronic manganese(II) cation to form dinuclear cryptates within the same host. The combination of three sp^2 N- and three O^--donors represents a relatively strong ligand field, and so raises the possibility of spin states other than $S = \frac{5}{2}$ for co-ordinated Fe^{III}.

Perchlorate, tetrafluoroborate and triflate salts of $[FeL^4]^{3+}$ were prepared to examine the influence of counter ion on iron(III) spin state. Comparison with earlier work[23,24] suggests that the nature of the anion is a significant factor in determining the position of equilibrium in $S = \frac{5}{2} \longleftrightarrow S = \frac{1}{2}$ spin crossover systems, and such an effect is not improbable here, given the likelihood of hydrogen bonding effects involving the protonated imino group. All the complexes show temperature-independent moments and a sensitivity of spin state to counter anion is observed (Table 1). Triflate and tetrafluoroborate[23a] salts show moments close to 5.9 μ_B, characteristic of the common high-spin $S = \frac{5}{2}$ configuration, while the moments of the perchlorate salts of both $[FeL^4]^{3+}$ and $[FeL^5]^{3+}$ are significantly lower, at 4.1 and 3.6 μ_B respectively, suggesting that the relatively rare intermediate ($S = \frac{3}{2}$) spin state is stabilised. In both **4a** and **5** the magnetic susceptibility, to a first approximation, follows Curie-law dependence down to 5 K, testifying to the absence of spin equilibrium effects over this wide temperature range. In **5** the observed moment could be considered as the consequence of the $S = \frac{3}{2}$ state with around 10% contribution from the $S = \frac{1}{2}$ form. Whether this arises from the presence of different spin states in the unit cell or from admixture of the low-lying doublet state into the quartet ground state[25] may not easily be decided, as Mössbauer relaxation rates for Fe^{III} are often so fast (*i.e.* $>10^7$ s^{-1}) that either extremely broadened or time-averaged[26] signals are seen for systems containing both high- and low-spin states. The observed anion dependence indicates that choice of ground state configuration is finely balanced for Fe^{III} within these cryptand hosts, *i.e.* that the $S = \frac{3}{2}$ and $\frac{5}{2}$ electronic states are relatively close in energy.

The spin quartet cryptates **4a** and **5** present weak Mössbauer spectra, requiring long acquisition times. The isomer shifts are close to those previously observed for $S = \frac{3}{2}$ iron(III) systems[26–28] although quadrupole splittings for **4a** and **5** are not as large as reported for the earlier, mainly square pyramidal, complexes. Presumably this is because the distortion stabilising the intermediate spin state, being trigonal in the cryptand structures, fails to generate a large electric field gradient. In the square pyramidal examples[26–28] a sizeable quadrupole splitting, which typifies the large electric field gradient associated with C_{2v} symmetry, accompanies stabilisation of the intermediate spin state. In the case of **5** no quadrupole splitting can be discerned in the very broad signal observed which testifies to rapid relaxation of spin on the Mössbauer time-scale. It seems possible that exchange of spin between singlet and quartet states is involved as the relaxation problem is more pronounced at 80 K than at room temperature, in contrast to the normal behaviour, shown in **4a**, where the quadrupole-split doublet is sharper at liquid nitrogen temperature. The reported isomer shifts for **5** are subject to large uncertainty on account of the breadth of the signal.

The polycrystalline ESR spectra of the spin-quartet systems

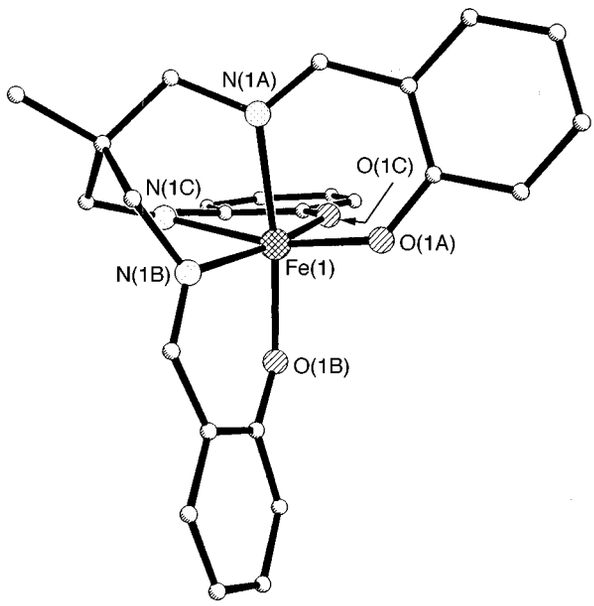

Fig. 3 Perspective view of $[FeL^6]$ **6**: only one of the two independent complexes is shown. Hydrogen atoms omitted for clarity

4a and **5** at 80 K show medium to high intensity features around $g \approx 4$ and ≈ 7 with a weaker, very broad signal at $g \approx 2$. The crystal structure of the perchlorate cryptate, **4a**, reported earlier, shows[9] distortion away from regular octahedral geometry in that the trigonal twist angle (40°) lies intermediate between trigonal prismatic (0) and octahedral (60°) values. The high-spin cryptate $[FeL^4][BF_4]_3 \cdot 6H_2O$ **4b** shows broad features at low field $g \approx 6$–7 and close to $g = 4$, together with a strong $g \approx 2$ signal.

Monoiron(III) complexes of podand and polydentate ligands

Where iminophenolate hosts other than cryptands are employed, *e.g.* podands or polydentate chelates, steric constraint is reduced or removed. The tren-capped podands such as substituted saltren (L^9) ligands have been studied[29,30] and exhibit co-ordination of Fe^{III} in the $S = \frac{5}{2}$ spin state. To extend this comparison we have made the tighter-capped L^6, which in the manganese series[9] has been shown to stabilise the +4 redox state and the crystal structure of the complex $[FeL^6] \cdot 0.75MeCN \cdot 0.125H_2O$ (**6**·0.75MeCN·0.125H_2O) has been determined. The asymmetric unit contains two independent but very similar $[FeL^6]$ complexes, one of which is shown in Fig. 3. The Fe–O^- and Fe–N distances (Table 3) were reduced (by *ca.* 0.1 and 0.2 Å respectively) in comparison with those in the analogous cryptate **4a**. The trigonal twist angles in the pair of independent molecules in the unit cell are ≈ 51 and ≈ 49°, *i.e.* about 10° from the regular octahedral angle of 60°, but not so far as in the iron(III) and manganese(II) cryptates. The average metal–ligand distances, compared with those of high-spin forms of $S = \frac{5}{2} \longleftrightarrow S = \frac{1}{2}$ spin crossover systems,[24a] are slightly (0.02 Å) reduced.

Despite the shorter iron(III)–ligand distances, magnetic moments show that the podate retains the high-spin $S = \frac{5}{2}$ iron(III) configuration shown in its tren-capped analogue. The ESR spectrum of complex **6** indicates rhombic distortion from octahedral symmetry, in that the dominant feature is an intense $g \approx 4$ signal. The high-spin iron(III) complexes **6** and **4b** show small (sometimes unresolved) to medium quadrupole splitting and atypically low Mössbauer isomer shifts, which may arise from covalency in the iron–ligand bonds; the short iron–ligand distances revealed in the structurally characterised podate **6** support this idea.

Moving to even less constrained polychelates of the hexadentate azaphenolates L^7 and L^8 there is a tendency to adopt a low-

Table 4 Comparison of geometric data for iron(III) and manganese complexes with iminophenolate ligands L^4, L^5, L^6 and L^9

	$[FeL^4]^{3+}$ **4a** (ref. 9)	$[MnL^4]^{2+}$ (ref. 9)	$[MnL^5]^{2+}$ (ref. 9)	$[FeL^9]$ (ref. 30)	$[MnL^9]$ [refs. 4(b) and 33]	$[MnL^6]^+$ (ref. 9)	$[FeL^6]$ **6**	
Redox state	+III	+II	+II	+III	+III	+IV	+III	
Space group	$R\bar{3}$	$P\bar{1}$	$P2_1/n$	$P2_1/c$	$P2_1/n$	Cc	$P\bar{1}$	-
M–O/Å	2.039(7)	2.029(5)	2.133(7)	1.940(1)	1.893(3)	1.853(2)	1.936(2)	1.945(2)
		2.101(4)	2.135(8)	1.965(1)	1.902(3)	1.868(1)	1.957(2)	1.940(2)
		2.194(4)	2.294(9)	1.976(1)	2.117(4)	1.881(2)	1.938(2)	1.947(2)
M–N/Å	2.343(8)	2.332(5)	2.256(9)	2.169(1)	2.051(4)	1.985(2)	2.147(2)	2.160(3)
		2.356(5)	2.294(8)	2.175(1)	2.083(4)	1.995(2)	2.143(2)	2.132(2)
		2.419(6)	2.294(9)	2.209(1)	2.327(4)	1.997(2)	2.159(2)	2.156(2)
Σ (deviations from 90°)[a]	140	129	123	56	59	20	72	73
O···O/Å	2.71	2.80	2.76	2.75	2.67	2.62	2.85	2.83
		2.81	2.78	2.78	2.77	2.68	2.88	2.84
		2.83	2.79	2.90	3.02	2.72	2.92	2.88
N···N/Å	3.75	3.57	3.55	3.14	3.13	2.72	2.79	2.86
		3.64	3.60	3.35	3.15	2.73	2.85	2.82
		3.75	3.63	3.36	3.45	2.77	2.87	2.88
Interplanar distance/Å	2.22	2.42	2.37	2.19	2.18	2.26	2.40	2.43
Interplanar angle[b]/°	0	3	2	6	8	1	1	1
Twist angle φ/°	40.3	36.0	43.5	59.0	61.5	58.3	50.7	48.3
		38.4	44.9	62.3	62.0	58.8	51.1	48.5
		39.3	45.2	63.2	64.1	59.5	51.1	48.9

[a] Sum of the deviation from 90° of the twelve *cis* angles in the co-ordination sphere. [b] Angle between the N_3 and $(O^-)_3$ planes.

spin $S = \frac{1}{2}$ ground state in Fe^{III}. This has already been noted[24b,31] for L^{10} as for the nitrate salt of L^7 and is here confirmed for the triflate salt $[FeL^7][CF_3SO_3]$ **7**, whose magnetic moment corresponds to one unpaired spin. The complex of the sterically hindered azaphenolate L^8 $[FeL^8][ClO_4]\cdot 3H_2O$ **8** shows a temperature-dependent moment suggesting the existence of a spin-crossover equilibrium between $S = \frac{5}{2}$ and $\frac{1}{2}$ spin states. The co-ordination geometry in **7** and **8** is presumably similar to that reported for analogous low-spin chelates of L^{10} and L^7 which have been structurally characterised.[24a,29a] These complexes exhibit axially contracted tetragonal geometry with metal–ligand distances of the order of 1.88 Å for Fe–O^- and 1.96–2.0 Å for Fe–N distances; *i.e.* over 0.05 Å shorter than Fe–O^- and 0.15 Å shorter than Fe–N in the podate **6**, in consequence of the smaller radius of the $S = \frac{1}{2}$ spin state of Fe^{III}. Such short co-ordination distances are not available within the phenolate cryptands, which is one reason for their choice of $S = \frac{5}{2}$ or $\frac{3}{2}$ ground states.

Complexes of the hexadentate polychelate ligand L^7 have, as reported earlier for other salts of such ligands,[24b,31] magnetic moments somewhat above the spin only value for the $S = \frac{1}{2}$ configuration, due to an orbital contribution which makes the moments slightly temperature dependent (*i.e.* 1.8–2.2 μ_B) over the temperature range 80–300 K. Their ESR spectra are typical of low-spin Fe^{III}, showing the characteristic set of three sharp resonances[32] around $g = 2$. The Mössbauer spectrum of complex **7** shows the expected large quadrupole splitting together with the small isomer shift typical of the low-spin iron(III) configuration.

The complex $[FeL^8][ClO_4]\cdot 3H_2O$ **8** is the only spin-crossover system to be studied, its moment decreases from ≈ 4.10 μ_B at 300 K to ≈ 2.86 μ_B at 4.2 K. At 160 K the ESR spectrum is still dominated by high-spin features, including an intense $g \approx 2$ and much weaker $g \approx 4$ signals. The room temperature Mössbauer spectrum (Fig. 4) presents two pairs of doublets, the minor intensity one having parameters characteristic of low-spin Fe^{III}. At 77 K this widely spaced quadrupole-split doublet becomes the major component of the spectrum, though the smaller quadrupole-split doublet corresponding to the high-spin isomer is still appreciable. These observations confirm the magnetic susceptibility data which suggest a very gradual change from high- to low-spin configuration on reducing temperature. The $S = \frac{5}{2}$ doublet is around 30% broader than the $S = \frac{1}{2}$ doublet, indicating faster relaxation in the high-spin configuration.

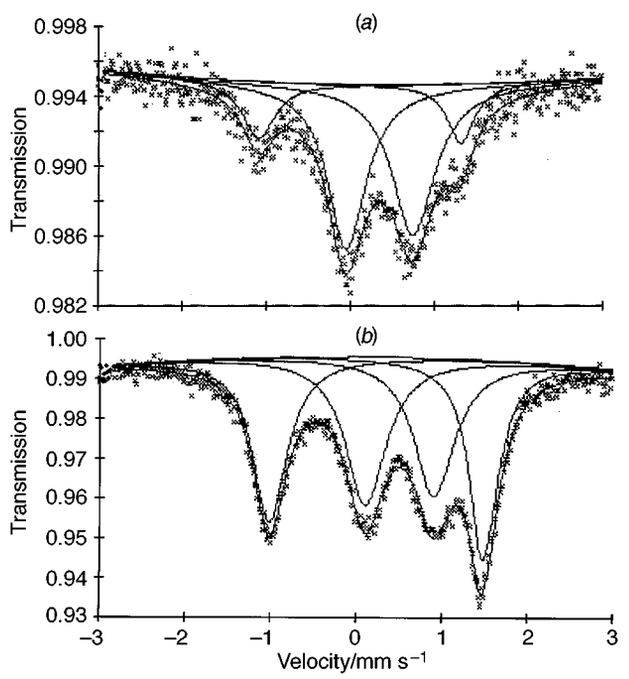

Fig. 4 Temperature dependence of the Mössbauer spectrum for complex **8**: (*a*) 300, (*b*) 77 K

Conclusion

Table 4 summarises the co-ordination geometry for the series of $N_3(O^-)_3$ iminophenolate cryptates and podates. The twist angle (φ) gives an indication of the trigonal distortions; a φ angle of 0° indicates trigonal prismatic geometry while a regular octahedron has φ = 60°. A general measure of the angular deviations from octahedral geometry is given by Σ; as expected, large values are best tolerated by the spherical iron(III) and manganese(II) high-spin ions. In some of the complexes investigated, spin states and, to some extent, oxidation states differ from those expected from consideration of the number and type of donors. These observations can be rationalised by consideration of the steric constraints imposed by the cryptand and podand ligands.

The mismatch between cavity size and ionic radius in the iron(II) complex of L^1 maintains **1** in the high-spin state, in spite

of the pyridine/imine donor set which might be expected to favour low spin. There is no very significant trigonal distortion in this complex but the irregular geometry also favours the high-spin form ($\Sigma = 101°$, mean $\varphi = 51°$ for **1**, compared to 64 and 54° for $[FeL^{11}](PF_6)_2$], the low-spin podate analogue[16]).

In iminophenolate cryptates both the size of the cavity and the extent of trigonal distortion enforced by ligands L^4 and L^5 are significant. In these systems the energies of the $\frac{5}{2}$ and $\frac{3}{2}$ states are finely balanced and the spin state adopted is influenced by the counter ion. In the iminophenolate podates formed by L^6 and L^9 the metal–ligand bonds are shorter than in the cryptates, there is significantly less trigonal distortion and Fe^{III} remains high spin.

Comparison of the iron(III) and manganese(IV) complexes of the small tris(aminomethyl)ethane (tame)-capped iminophenolate podand L^6 shows, as expected, that the manganese(IV) complex has shorter bonds and less distortion than the analogous iron(III) podate. Indeed, even the tren-capped manganese(III) podate [MnL^9] shows somewhat shorter metal–ligand distances than those of **6**. In contrast the iron(III) L^9 analogue has Fe–N and Fe–O^- distances[30] very slightly longer than those of **6** but shows considerably less trigonal distortion. Notwithstanding the Mössbauer evidence of greater covalent character in **6**, the high-spin state is stabilised rather than $S = \frac{1}{2}$ as in the relatively unconstrained hexadentate chelates, or $S = \frac{3}{2}$ as in the cryptates.

These observations corroborate the critical role of geometry in control of spin state.

Experimental

Synthesis

$[FeL^1][ClO_4]_2$ 1. To a $CHCl_3$–MeCN–EtOH (40:40:10) solution of L^1 (1 mmol in 100 cm^3) prepared as described elsewhere[34] was added solid hydrated iron(II) perchlorate (1 mmol) at room temperature. A brownish pink solid was obtained in 62% yield. It is important to isolate this product quickly to avoid contamination with the blue-purple impurity. Crystals of **1**·MeCN were obtained by diffusion of diethyl ether into an acetonitrile solution of the complex [Found (Calc.): C, 46.92 (46.94); H, 4.83 (4.66); N, 17.86 (18.25)%]. FAB mass spectrum: *m*/*z* (% basepeak) $FeL(ClO_4)$, 744 (82); FeL, 645 (100). Selected IR: $\tilde{\nu}_{max}/cm^{-1}$ 3421, 2851, 1652, 1596, 1461, 1122, 1093, 1047 and 623.

$[Fe_2(N_3)L^2]X_3\cdot 2H_2O$ (X = CF_3SO_3 2a or ClO_4 2a′). A solution of the iron(II) salt [0.2 mmol in EtOH–MeCN (2:1, 15 cm^3)] was added to a deoxygenated solution of L^2 [0.1 mmol in MeOH–MeCN (1:1, 15 cm^3)] made as described elsewhere.[35] The solution was stirred at 40 °C for a couple of minutes before addition of NaN_3 (0.1 mmol) in a few drops of water. The mixture was stirred for 2 h before filtering to isolate the light tan product in 26 (for **2a**) to 50% (for **2a′**) yield [Found (Calc.): **2a**, C, 37.23 (37.90); H, 4.11 (4.73); N, 12.21 (12.47). **2a′**, C, 39.99 (39.77); H, 5.56 (5.28); N, 13.53 (14.17)%]. FAB mass spectrum: *m*/*z* (% basepeak) **2a**, FeL, 653 (37); $FeL(CF_3SO_3)$, 803 (10); $Fe_2N_3L(CF_3SO_3)_2$, 1050 (100); **2a′**, FeL, 651 (15); $Fe_2LN_3(ClO_4)$, 850 (30); $Fe_2N_3L(ClO_4)_2$, 950 (100). Selected IR: $\tilde{\nu}_{max}/cm^{-1}$ **2a**, 3439, 3227, 2915, 2192, 1629, 1466, 1443, 1328, 1277, 1197, 1161, 1029, 794, 754 and 638.

$[Fe_2(OH)L^2][PF_6]_3\cdot 4H_2O$ 2b. A deoxygenated solution of $Fe(CF_3SO_3)_2\cdot 6H_2O$ (0.8 mmol) in EtOH–MeCN (2:1, 15 cm^3) was added to L^2 (0.4 mmol) in deoxygenated EtOH–MeCN (1:1, 20 cm^3) and the mixture stirred at 40 °C for 20 min before ammonium hexafluorophosphate was added as a solid. After stirring at this temperature for 15 min a cream precipitate started to appear, which was filtered off after sitting in ice for 30 min. Yield 16% [Found (Calc.): C, 34.86 (35.04); H, 5.04 (4.98); N, 8.89 (9.08)%]. FAB mass spectrum: *m*/*z* (% basepeak) H_2L, 600 (100); FeL, 654 (17). Selected IR: $\tilde{\nu}_{max}/cm^{-1}$ 3428, 3275, 2926, 2879, 1613, 1470, 1448, 1434, 1282, 1164, 1068, 1027, 924, 842 and 556.

$[Fe_2(OH)L^3][CF_3SO_3][BPh_4]_2$ 3. Iron(II) triflate (0.2 mmol) dissolved in deoxygenated EtOH–MeCN (2:1, 15 cm^3) was added to L^3 (0.1 mmol), made as described elsewhere,[11a] in EtOH–MeCN (1:1, 15 cm^3). Sodium tetraphenylborate (0.5 mmol) in EtOH (20 cm^3) was added after 5 min stirring at 40 °C. After 1 h of cooling in ice the product was isolated by filtration under nitrogen. Yield 18% [Found (Calc.): C, 63.23 (63.90); H, 5.87 (6.04); N, 7.67 (7.55)%]. Selected IR: $\tilde{\nu}_{max}/cm^{-1}$ 3509, 3277, 3048, 2993, 1574, 1473, 1445, 1274, 1264, 1232, 1179, 1023, 1008, 971, 959, 734 and 706.

$[FeL^4][ClO_4]_3\cdot 0.5MeCN$ 4a. To $[NaL^4][ClO_4]$ (0.5 mmol), prepared as described elsewhere,[11b] in acetonitrile–chloroform solvent (1:1, 40 cm^3), was added solid iron(III) perchlorate decahydrate (1 mmol). This caused an immediate change to deep green-black. After stirring for 15 min at room temperature the dark green solid was filtered off in 26% yield [Found (Calc.): C, 46.84 (45.69); H, 4.94 (4.74); N, 11.50 (11.32)%]. FAB mass spectrum: *m*/*z* (% basepeak): FeL, 731 (35); $FeL(ClO_4)$, 930 (4). Selected IR: $\tilde{\nu}_{max}/cm^{-1}$ 3440, 2930, 2870, 1655, 1555, 1535, 1480, 1450, 1355, 1300, 1220, 1160, 1090, 1040, 990, 880 and 630.

$[FeL^4]X_3\cdot xH_2O$ (X = BF_4, x = 6 4b; X = CF_3SO_3, x = 3 4c). These complexes were prepared analogously to **4a**, using the appropriate iron(II) salt [Found (Calc.): **4b**, C, 43.46 (43.26); H, 5.57 (5.41); N, 10.32 (9.82). **4c**, C, 41.10 (40.88); H, 4.02 (4.41); N, 8.79 (9.08)%].

$[FeL^5][ClO_4]_3\cdot EtOH$ 5. A solution of tris(2-aminoethyl)-amine (tren) [2 mmol in MeCN–EtOH (2:3, 25 cm^3)] was added dropwise to an ethanolic solution of 4-*tert*-butyl-2,6-diformylphenol (3 mmol, 20 cm^3) and sodium perchlorate (1 mmol), causing a red colour to develop. Solid $Fe(ClO_4)_3\cdot 6H_2O$ (1 mmol) was then added and the deep green solution allowed to stir for 15 min before being filtered and allowed to stand in air to crystallise. Yield 34% [Found (Calc.): C, 50.17 (49.91); H, 6.26 (6.03); N, 9.70 (9.31)%]. FAB mass spectrum: *m*/*z* (% basepeak) FeL, 857 (15); HL, 804 (26). Selected IR: $\tilde{\nu}_{max}/cm^{-1}$ 3440, 2930, 2870, 1655, 1555, 1535, 1480, 1450, 1355, 1300, 1220, 1160, 1090, 1040, 990, 880 and 630.

$[FeL^6]\cdot 0.75MeCN\cdot 0.125H_2O$ 6·0.75MeCN·0.125H_2O. Tris-(aminomethyl)ethane (3 mmol) in MeCN–EtOH (1:1, 30 cm^3) was added dropwise to a solution of salicylaldehyde (9 mmol) in an equal volume of the same solvent mixture, causing development of a bright yellow colour. Addition of solid iron(II) perchlorate then caused a change to deep maroon, and the product was isolated on reducing the volume as crystals suitable for X-ray studies. Yield 57% [Found (Calc.): C, 64.09 (63.97); H, 5.18 (4.88); N, 10.19 (9.24)%]. FAB mass spectrum: *m*/*z* (% basepeak) FeL, 483 (100). Selected IR: $\tilde{\nu}_{max}/cm^{-1}$ 3436, 3047, 3020, 2905, 1622, 1597, 1541, 1469, 1444, 1396, 1339, 1311, 1200, 1150, 897, 798, 762 and 604.

$[FeL^7][CF_3SO_3]$ 7. 4,7-Diazadecane-1,10-diamine (3 mmol) dissolved in EtOH–MeCN (1:1, 30 cm^3) was added dropwise to salicylaldehyde (6 mmol) in an equal volume of the same solvent mixture. On addition of the appropriate iron salt as a solid a bright purple colour developed, and the solid was isolated on reducing the volume. Yield 47% [Found (Calc.): C, 46.85 (47.19); H, 4.46 (4.82); N, 9.28 (9.57)%]. FAB mass spectrum: *m*/*z* (% basepeak) FeL, 435 (100). Selected IR: $\tilde{\nu}_{max}/cm^{-1}$ 3446, 2917, 2860, 1651, 1619, 1544, 1472, 1406, 1340, 1314, 1278, 1224, 1202, 1152, 1031, 931, 893, 761, 738 and 638 cm^{-1}.

$[FeL^8][ClO_4]\cdot 3H_2O$ 8. This product was prepared analogously to chelate **7** using triethylenetetramine (trien) with 2-

hydroxynaphthalaldehyde in place of salicylaldehyde followed by recrystallisation from MeCN–EtOH. Yield 32% [Found (Calc.): C, 51.3 (50.9); H, 4.8 (5.0); N, 8.5 (8.5)%]. FAB mass spectrum: *m/z* (% basepeak) FeL, 508 (100). Selected IR: $\tilde{\nu}_{max}$/cm^{-1} 3726m, 3056m, 2936m, 1616s, 1603s, 1541, 1359, 1342, 1083, 829, 763, 751 and 622. Some preparations of this complex showed FAB peaks corresponding to the $Fe_2L_2(ClO_4)_2$ dimer formulation.

Crystallography

Crystal data. $[FeL^1][ClO_4]_2$·MeCN, **1**·MeCN, $C_{35}H_{42}Cl_2FeN_{12}O_8$, triclinic, space group $P\bar{1}$, $a = 10.9262(1)$, $b = 13.3979(2)$, $c = 14.7728(2)$ Å, $\alpha = 71.7616(1)$, $\beta = 80.5016(4)$, $\gamma = 70.4503(1)°$, $U = 1931.12(4)$ Å^3, $T = 160(2)$ K, $Z = 2$, $\mu = 0.598$ mm^{-1}. Data for a crystal of dimensions $0.08 \times 0.06 \times 0.04$ mm were collected using a Siemens SMART CCD diffractometer with synchrotron radiation ($\lambda = 0.6879$ Å, SRS station 9.8 at Daresbury Laboratory). 11 648 Reflections were collected, corrected for Lorentz-polarisation effects and for the decay of the incident beam. 8022 Independent reflections ($R_{int} = 0.0655$), $wR(F^2) = 0.1564$, conventional $R = 0.0652$ (data with $F^2 > 2\sigma$).

$[FeL^6]$·0.75MeCN·0.125H_2O **6**·0.75MeCN·0.125H_2O, $C_{27.5}H_{26.5}FeN_{3.75}O_{3.13}$, triclinic, space group $P\bar{1}$, $a = 11.010(2)$, $b = 14.127(2)$, $c = 16.284(2)$ Å, $\alpha = 93.69(1)$, $\beta = 102.92(1)$, $\gamma = 98.12(1)°$, $U = 2431.8(6)$ Å^3, $T = 150(2)$ K, $Z = 4$, μ(Mo-Kα) = 0.658 mm^{-1}, 9033 reflections measured, 8551 independent ($R_{int} = 0.0198$) and used in all calculations. Final $R'(F^2) = 0.0883$, conventional $R = 0.0381$ (data with $F^2 > 2\sigma$). All programs used in the structure solutions and refinements are contained in the SHELXL 97 package.[36]

CCDC reference number 186/971.

See http://www.rsc.org/suppdata/dt/1998/1837/ for crystallographic files in .cif format.

Physical measurements

The Mössbauer effect experiments were carried out at room temperature and liquid nitrogen temperature using a commercial constant acceleration spectrometer (Harwell Instruments). The source used was 10 mCi (nominal) of ^{57}Co in Rh. All isomer shift values are with reference to iron metal. The data were analysed using a non-linear curve-fitting program. The ESR and magnetic measurements (SUP 57377) were made as described[5,20] in earlier papers.

Acknowledgements

We thank EPSRC for access to the FAB mass spectrometry service at Swansea, the Open University Research Committee for support (to G. G. M.) and EPSRC for access to the Synchrotron Radiation Source, Station 9.8 at CLRC, Daresbury.

References

1 See, for example, M. M. Bishop, J. Lewis, T. D. O'Donoghue, P. R. Raithby and J. N. Ramsden, *J. Chem. Soc.*, *Dalton Trans.*, 1980, 1390; S. M. Nelson, P. Bryan and D. H. Busch, *Chem. Commun.*, 1966, 641; S. M. Nelson and D. H. Busch, *Inorg. Chem.*, 1969, **8**, 1859; B. F. Hoskins, R. Robson and G. A. Williams, *Inorg. Chim. Acta*, 1976, **16**, 121.
2 D. R. Boston and N. J. Rose, *J. Am. Chem. Soc.*, 1968, **90**, 6859.
3 N. Herron, M. Y. Chavan and D. H. Busch, *J. Chem. Soc.*, *Dalton Trans.*, 1984, 1491.
4 (*a*) R. J. Motekaitis, A. E. Martell and W. Benutely, *Inorg. Chim. Acta*, 1993, **205**, 23; (*b*) G. Morgan, Ph.D. Thesis, Open University, 1995.
5 M. G. B. Drew, J. Hunter, D. J. Marrs, J. Nelson and C. J. Harding, *J. Chem. Soc.*, *Dalton Trans.*, 1992, 3235.
6 J. Hunter, Ph.D. Thesis, Open University, 1991.
7 S. J. Lippard, *Angew. Chem.*, *Int. Ed. Engl.*, 1988, **27**, 344.
8 K. N. Raymond, T. J. McMurry and T. M. Garrett, *Pure Appl. Chem.*, 1988, **60**, 545; K. N. Raymond and T. M. Garrett, *Pure Appl. Chem.*, 1988, **60**, 1807.
9 M. G. B. Drew, C. J. Harding, G. G. Morgan, V. McKee and J. Nelson, *J. Chem. Soc.*, *Chem. Commun.*, 1995, 1035.
10 P. Gutlich, A. Hauser and H. Speiring, *Angew. Chem.*, *Int. Ed. Engl.*, 1994, **33**, 2024; P. Gutlich and A. Hauser, *Coord. Chem. Rev.*, 1990, **97**, 1.
11 See, for example, (*a*) Q. Lu, J.-M. Latour, C. J. Harding, N. Martin, D. Marrs, V. McKee and J. Nelson, *J. Chem. Soc.*, *Dalton Trans.*, 1994, 649; (*b*) M. G. B. Drew, O. Howarth, G. G. Morgan and J. Nelson, *J. Chem. Soc.*, *Dalton Trans.*, 1994, 3149; (*c*) G. G. Morgan, V. McKee and J. Nelson, *Inorg. Chem.*, 1994, **33**, 4427 and refs. therein.
12 J. Hunter, C. J. Harding, M. McCann, V. McKee and J. Nelson, *J. Chem. Soc.*, *Chem. Commun.*, 1990, 1148 and refs. therein.
13 Q. Lu, C. J. Harding, V. McKee and J. Nelson, *Inorg. Chim. Acta*, 1993, **211**, 195.
14 R. Abidi, F. Arnaud-Neu, M. G. B. Drew, S. Lahely, D. J. Marrs, J. Nelson and M.-J. Schwing-Weil, *J. Chem. Soc.*, *Perkin Trans. 2*, 1996, 2747.
15 N. N. Greenwood and T. C. Gibb, *Mössbauer Spectroscopy*, Chapman and Hall, London, 1971.
16 L. J. Wilson and N. J. Rose, *J. Am. Chem. Soc.*, 1968, **90**, 6041; C. Mealli and E. C. Lingafelter, *J. Chem. Soc. D*, 1970, 885; K. Boubeker, A. Deroche, F. Lambert and I. Morgenstern-Badarau, *Acta Crystallogr.*, *Sect. C*, 1995, **51**, 2244.
17 E. B. Fleischer, A. E. Gebala, D. R. Swift and P. A. Tasker, *Inorg. Chem.*, 1972, **11**, 2775.
18 See, for example, M. G. B. Drew, M. McCann and S. M. Nelson, *Inorg. Chim. Acta*, 1980, **41**, 213; C. Cairns, S. M. Nelson and M. G. B. Drew, *J. Chem. Soc.*, *Dalton Trans.*, 1981, 1965; L. Mazzarella, C. Pellecchia, C. A. Mattia, V. de Felice and R. Puliti, *J. Coord. Chem.*, 1986, **14**, 191; I. Vasilevsky, R. E. Stenkamp, E. C. Lingafelter and N. J. Rose, *J. Coord. Chem.*, 1988, **19**, 171; C. Piguet, G. Bernardinelli, A. F. Williams and B. Bocquet, *Angew. Chem.*, *Int. Ed. Engl.*, 1995, **34**, 582; C. Scheer, P. Chautemps, I. Gautier-Luneau, J.-L. Pierre, G. Serratrice and E. Saint-Aman, *Polyhedron*, 1996, **15**, 219; S. Brooker and T. Simpson, *J. Chem. Soc.*, *Dalton Trans.*, 1998, 1151.
19 C. J. Harding, F. J. Mabbs, E. J. MacInnes, V. McKee and J. Nelson, *J. Chem. Soc.*, *Dalton Trans.*, 1996, 3227.
20 Q. Lu, C. J. Harding, V. McKee and J. Nelson, *J. Chem. Soc.*, *Dalton Trans.*, 1993, 1768.
21 W. H. Armstrong and S. J. Lippard, *J. Am. Chem. Soc.*, 1983, **105**, 4837; W. H. Armstrong, A. Spool, G. C. Papaefthymiou, R. B. Frankel and S. J. Lippard, *J. Am. Chem. Soc.*, 1984, **106**, 3653; P. Chaudhuri, K. Wieghardt, B. Nuber and J. Weiss, *Angew. Chem.*, *Int. Ed. Engl.*, 1985, **24**, 778.
22 Y. Dussart, A. Escuer, R. Vicente, C. J. Harding, J. Nelson and V. McKee, in preparation.
23 (*a*) W. M. Marrit, Ph.D. Thesis, Cal Tech., 1982; (*b*) M. D. Timken, W. A. Marritt, D. N. Hendrickson, R. A. Gagné and E. Sinn, *Inorg. Chem.*, 1985, **24**, 4203.
24 (*a*) E. Sinn, P. G. Sim, E. V. Dose, M. F. Tweedle and L. J. Wilson, *J. Am. Chem. Soc.*, 1978, **100**, 3375; (*b*) M. F. Tweedle and L. J. Wilson, *J. Am. Chem. Soc.*, 1976, **98**, 4824; (*c*) E. V. Dose, K. M. M. Murphy and L. J. Wilson, *Inorg. Chem.*, 1976, **15**, 2622.
25 M. M. Maltempo, *J. Chem. Phys.*, 1974, **61**, 2540; J. S. Griffith, *Mol. Phys.*, 1964, **8**, 213.
26 K. D. Hodges, R. G. Wollmann, S. L. Kessel, D. N. Hendrickson, D. G. Van Derveer and E. K. Barefield, *J. Am. Chem. Soc.*, 1979, **101**, 906; H. Mosbaek and K. G. Poulsen, *Acta Chem. Scand.*, 1971, **15**, 2421.
27 F. V. Wells, S. W. McCann, H. H. Wickman, S. L. Kessel, D. N. Hendrickson and R. D. Feltham, *Inorg. Chem.*, 1982, **21**, 2306.
28 H. Wickman and A. M. Trozzolo, *Inorg. Chem.*, 1968, **7**, 63.
29 (*a*) D. F. Cook, D. Cummins and E. D. McKenzie, *J. Chem. Soc.*, *Dalton Trans.*, 1976, 1369; (*b*) S. K. Chandra, P. Chakraborty and A. Chakravorty, *J. Chem. Soc.*, *Dalton Trans.*, 1993, 863.
30 Y. Elerman, M. Kabak, I. Svoboda, H. Fuess and O. Atakal, *J. Chem. Crystallogr.*, 1995, **25**, 227.
31 T. Ito, M. Sugimoto, H. Ito, K. Toriumi, H. Nakayama, W. Mori and M. Sakazaki, *Chem. Lett.*, 1983, 121.
32 R. S. Drago, *Physical Methods in Chemistry*, W. B. Saunders, Philadelphia, London, New York, 1977.
33 S. K. Chandra and A. Chakravorty, *Inorg. Chem.*, 1991, **30**, 3795.
34 M. G. B. Drew, V. Felix, G. Morgan, V. McKee and J. Nelson, *J. Supramol. Chem.*, 1995, **5**, 281.
35 J. Nelson and D. McDowell, *Tetrahedron Lett.*, 1988, 385; C. J. Harding, Q. Lu, D. J. Marrs, N. Martin, V. McKee and J. Nelson, *J. Chem. Soc.*, *Dalton Trans.*, 1995, 1739.
36 G. M. Sheldrick, SHELXL 97, University of Göttingen, 1997.

Received 5*th February* 1998; *Paper* 8/01046C